nature geoscience

ARTICLES

PUBLISHED ONLINE: 20 MAY 2012 | DOI: 10.1038/NGEO1478

Riverine source of Arctic Ocean mercury inferred from atmospheric observations

Jenny A. Fisher[1]*, Daniel J. Jacob[1,2], Anne L. Soerensen[2,3], Helen M. Amos[1], Alexandra Steffen[4] and Elsie M. Sunderland[2,3]

Methylmercury is a potent neurotoxin that accumulates in aquatic food webs. Human activities, including industry and mining, have increased inorganic mercury inputs to terrestrial and aquatic ecosystems. Methylation of this mercury generates methylmercury, and is thus a public health concern. Marine methylmercury is a particular concern in the Arctic, where indigenous peoples rely heavily on marine-based diets. In the summer, atmospheric inorganic mercury concentrations peak in the Arctic, whereas they reach a minimum in the northern mid-latitudes. Here, we use a global three-dimensional ocean–atmosphere model to examine the cause of this Arctic summertime maximum. According to our simulations, circumpolar rivers deliver large quantities of mercury to the Arctic Ocean during summer; the subsequent evasion of this riverine mercury to the atmosphere can explain the summertime peak in atmospheric mercury levels. We infer that rivers are the dominant source of mercury to the Arctic Ocean on an annual basis. Our simulations suggest that Arctic Ocean mercury concentrations could be highly sensitive to climate-induced changes in river flow, and to increases in the mobility of mercury in soils, for example as a result of permafrost thaw and forest fires.

Mercury is emitted from anthropogenic and natural sources primarily as elemental mercury (Hg^0). The Hg^0 atmospheric lifetime of 6–12 months allows transport of this emitted mercury on a hemispheric scale. Eventual oxidation to highly soluble Hg^{II} drives deposition in remote regions. Hg^0 has been measured continuously at sites across the Arctic since the mid-1990s (refs 1–3). As seen in Fig. 1, Hg^0 concentrations in surface air at high Arctic coastal sites exhibit a strong seasonality with minimum in spring and maximum in summer. This contrasts with observations at northern mid-latitudes that show a weak minimum in late summer due to destruction by photochemically produced oxidants[4]. The spring decrease in the Arctic reflects atmospheric mercury depletion events (AMDEs) initiated by the photochemical release of bromine radicals ($BrO_x \equiv Br + BrO$) from sea salt concentrated in sea ice[5]. High BrO_x concentrations drive rapid oxidation of Hg^0 to Hg^{II} (ref. 6) and subsequent deposition to snow and ice.

The summer maximum of Hg^0 in the Arctic atmosphere is less understood. It was initially attributed to re-emission of mercury deposited to snow and ice during spring[7]. Recent work has called this assumption into question[1], invoking instead an oceanic source[3,8,9]. Atmosphere–ocean Hg^0 exchange is expected to exhibit strong seasonality driven by variations in sea-ice cover, temperature, freshwater inputs and light availability. Arctic Ocean cruise data show elevated summertime concentrations of mercury both above and below sea ice[10–12], suggesting large fluxes of Hg^0 to the atmosphere from supersaturated ocean waters[12]. However, the mechanisms supplying the oceanic pool of Hg^0 subject to evasion have not been explained.

Seasonal variation of Arctic mercury

Figure 1 shows the mean observed seasonal cycle of atmospheric Hg^0 at three high Arctic sites: Alert (Canada), Amderma (Russia) and Zeppelin Mountain (Ny Ålesund, Norway). Concentrations vary in amplitude across the three sites but all show similar seasonality, with minimum in April–May and maximum in July. Autumn–winter concentrations at Arctic sites show no mean significant difference from northern mid-latitudes, reflecting the long mercury lifetime relative to the timescales for extratropical mixing.

We simulate the seasonal cycle of atmospheric mercury in the Arctic using the GEOS-Chem global mercury model, which includes a three-dimensional atmospheric transport and chemistry simulation[13] dynamically coupled to a two-dimensional ocean mixed layer simulation with redox chemistry and exchange with subsurface waters[14]. GEOS-Chem has been extensively evaluated with atmospheric and oceanic observations[13,14] and has been intercompared with other global and regional mercury models[15,16]. Relative to previous versions[13,14], the present implementation includes a new temperature-dependent scheme for bromine release from sea ice, an improved radiation-dependent treatment of mercury deposited to snow and updated Arctic-specific ocean parameters for vertical exchange (see Methods). The model does not include lateral transport in the surface ocean, limiting its ability to simulate horizontal gradients across the Arctic Ocean. We focus therefore on simulating the mean seasonal behaviour across the three Arctic sites.

Figure 2 compares the multi-year mean observed Hg^0 seasonal variation (black) with that simulated for 2008 by the standard GEOS-Chem model described above (red) and by including changes to various model parameters ('sensitivity simulations'). Simulated seasonality is insensitive to the choice of model year. The standard simulation accurately reproduces the spring decrease driven by AMDEs, which account for 60% of modelled deposition to the Arctic in spring. This largely reflects the assumed

[1]Department of Earth and Planetary Sciences, Harvard University, Cambridge, Massachusetts 02138, USA, [2]School of Engineering and Applied Sciences, Harvard University, Cambridge, Massachusetts 02138, USA, [3]Department of Environmental Health, Harvard School of Public Health, Harvard University, Boston, Massachusetts 02215, USA, [4]Air Quality Processes Research Section, Environment Canada, Toronto, Ontario M3H 5T4, Canada.
*e-mail: jafisher@fas.harvard.edu.

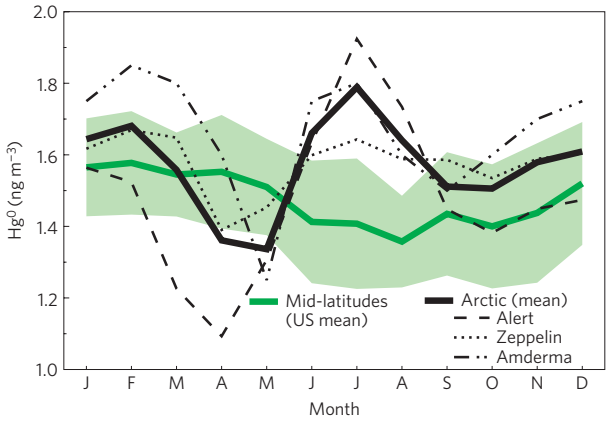

Figure 1 | Seasonal variation of atmospheric Hg^0. Monthly mean observed Hg^0 concentrations in surface air for the Arctic (solid black line) and US northern mid-latitudes (green line). Arctic values are an average over: Alert, Canada (83° N, 62° W; 2005–2009; ref. 1); Zeppelin Mountain, Norway (79° N, 12° E; 2000–2009; ref. 2); and Amderma, Russia (70° N, 62° E; 2001–2003; ref. 1); individual sites are shown as thin dashed/dotted lines. Values at mid-latitudes are an average over: Cheeka Peak, Washington (2001–2002; ref. 47); Pack Monadnock, New Hampshire (2007; ref. 48); Athens, Ohio (2004–2005; ref. 49); and Pensacola, Florida (2005–2008; ref. 13). The green shading indicates the standard deviation of monthly means among mid-latitude sites.

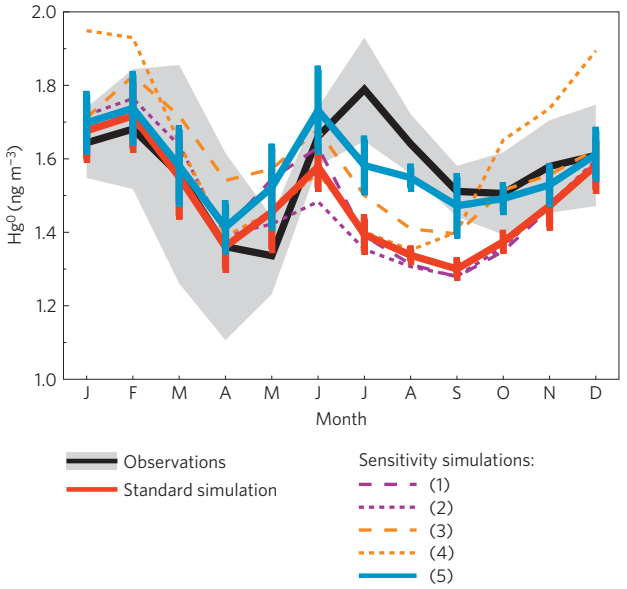

Figure 2 | Simulated seasonal variation of Hg^0 concentrations in Arctic surface air. Observations (black) are multi-year averages across the three Arctic sites of Fig. 1. Model results are averages over these sites in 2008 for the standard simulation (red) and the sensitivity simulations described in the text: (1) increased reducible percentage of mercury in snow (purple dashed); (2) increased in-snow reduction rate (purple dotted); (3) increased ratio of photo-reduction to photo-oxidation (orange dashed); (4) increased biotic reduction rate (orange dotted); and (5) input of riverine and erosional Hg^{II} to the ocean (blue). The standard deviation among sites is indicated by grey shading for the observations and vertical bars for the simulations.

dependences of BrO on temperature and of snowpack re-emission on solar radiation (see Methods). Fifty per cent of the mercury deposited in AMDEs is re-emitted to the atmosphere in the model, but the net sink is enough to drive a 20% decrease in Hg^0 over the Arctic in spring, consistent with observations (Fig. 2).

We see from Fig. 2 that the standard simulation fails to reproduce the observed summer maximum. It shows only a weak peak in June driven by re-emission from snow, followed by a July–September decrease due to uptake by the ocean. The summer underestimate cannot be explained by a missing atmospheric source from mid-latitudes because observed summer mercury concentrations shown in Fig. 1 are much higher in the Arctic than at mid-latitudes. The Arctic must therefore be a net atmospheric exporter of mercury rather than importer in summer. This is consistent with statistical analysis of observations at Zeppelin showing that high concentrations are associated with transport from mid-latitudes in winter and spring but not in summer[8]. Atmospheric redox chemistry is also unable to explain the model underestimate in summer as Hg^{II} accounts for <2% of total Arctic gas-phase mercury both in the model and in observations[11,17].

We investigated whether the summer peak could be driven by re-emission of mercury deposited to the Arctic cryosphere in spring. Observational constraints on in-snow reduction and re-emission of deposited mercury show large uncertainties[18]. We performed sensitivity simulations for both continental and sea-ice snow with (simulation 1) the reducible percentage of mercury in snow increased from 60% in the standard model[13] to 90% (an upper limit from observations[19]) and (simulation 2) the net in-snow reduction rate constant increased by a factor of 100 (consistent with the spread of observational estimates[18], see Methods). Results shown in Fig. 2 (purple) indicate negligible impact on either the timing or the magnitude of the summer peak. This is because re-emission can take place only in a narrow seasonal window between the onset of radiation (April) and the onset of snowmelt (May–June), when dissolved mercury is rapidly eluted from the snowpack during an ionic pulse lasting only a few days[18]. When the snowpack reduction rate is increased, the snowpack becomes depleted earlier and atmospheric concentrations in June are actually lower than in the standard simulation. When the snowpack reduction rate is decreased, the snow mercury reservoir is removed with the melt water before re-emission can occur.

Mercury added to the ocean mixed layer may be re-emitted to the atmosphere by reduction of dissolved Hg^{II} to Hg^0 or transferred to the subsurface ocean by wind-driven mixing and particle settling. Figure 3a shows the modelled seasonal budget of total mercury ($THg \equiv Hg^0 + Hg^{II}$; see Methods) in the ocean mixed layer, with inputs (melt water, entrainment from subsurface waters and atmospheric deposition) in red and outputs (evasion, detrainment to subsurface waters and particle settling) in blue. Removal from the mixed layer to subsurface waters peaks during spring and summer, when stratification drives shoaling of the mixed layer[20,21] and increased biological productivity enhances losses associated with settling particles[22]. These losses to the subsurface ocean exceed atmospheric inputs from direct deposition and meltwater delivery, both in the standard simulation and in a sensitivity simulation with the particle settling flux substantially reduced (see Supplementary Information). The modelled summer minimum in Arctic Ocean mixed layer THg is 1.1 pM, much lower than the 2.8 pM mean of August–October observations from surface waters of the Canadian Arctic[23].

The modelled reservoir of THg in the surface ocean is too small for large evasion fluxes in summer to be driven solely by enhanced reduction of Hg^{II} to Hg^0. Model sensitivity studies confirm that despite observed Hg^0 supersaturation of up to 1,800% below sea ice[12], the reducible pool of Hg^{II} (and associated evasion) is rapidly depleted without further external inputs. We performed a sensitivity simulation (simulation 3) increasing the rate of photo-reduction (generally the main pathway for Hg^{II} reduction in the ocean mixed layer[14]) and decreasing the rate of photo-oxidation in the Arctic Ocean both by a factor of five, representing an extreme

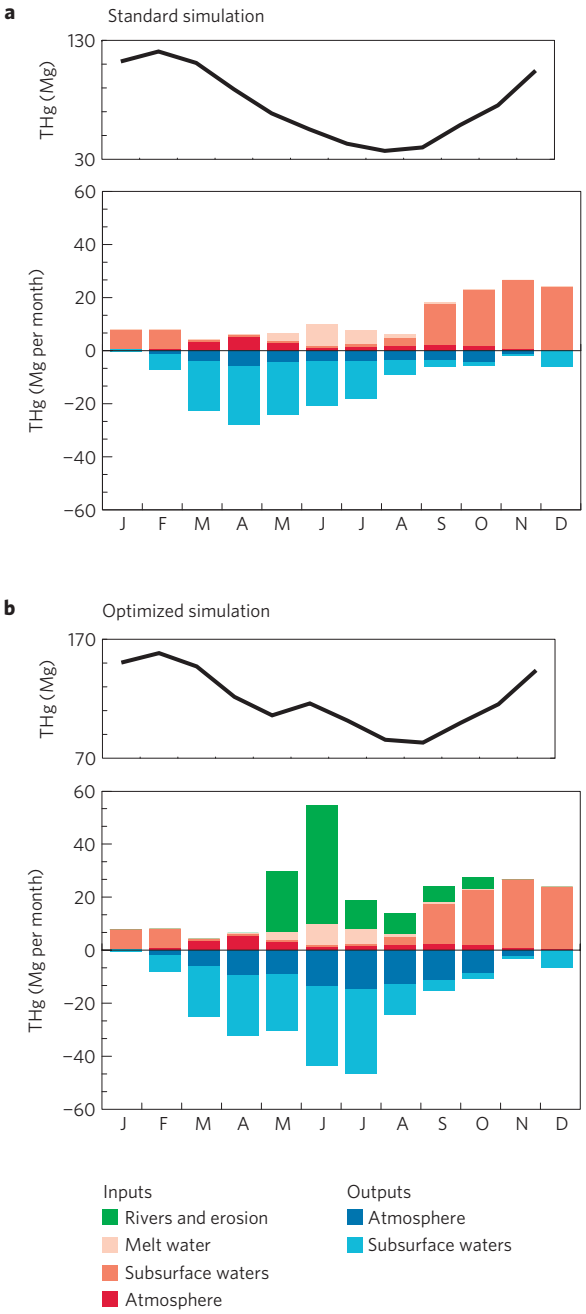

Figure 3 | Seasonal budget of mercury in the Arctic Ocean mixed layer (70°–90° N). a,**b**, The masses and fluxes of THg in the standard simulation (**a**) and the optimized simulation including riverine and erosional inputs (**b**). The solid black lines show the seasonal variation of THg mass in the ocean mixed layer. Inputs (red and green) include the sources from rivers and erosion, melt water, subsurface waters through entrainment and the atmosphere through Hg^{II} deposition. Outputs (blue) include removal to the atmosphere through net Hg^0 evasion and to the subsurface ocean through detrainment and settling particles.

perturbation. Figure 2 (orange dashed line) shows that the model still cannot sustain a summer maximum even under such unlikely photo-redox conditions.

In coastal Arctic environments, biologically mediated reduction by mercury-resistant microbes can be a dominant source of Hg^0 even at cold temperatures[24]. As this reduction pathway is independent of light availability, it can operate in winter and below sea ice and has therefore been suggested as a major driver

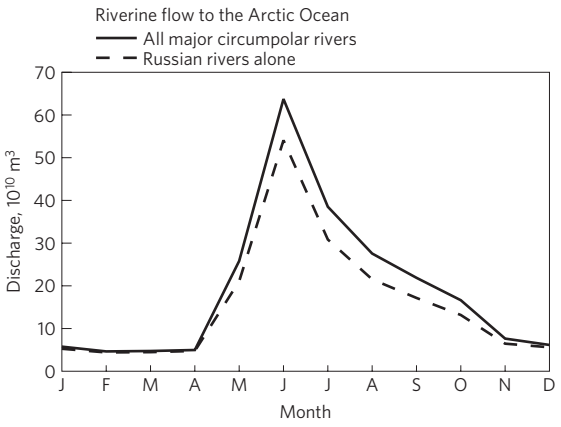

Figure 4 | Mean seasonal variation of river discharge into the Arctic Ocean. Water discharge is summed over the eight largest circumpolar rivers (solid line) including the Yenisei, Lena, Ob, Pechora, Dvina and Kolyma in Russia and the Mackenzie and Yukon in North America. The dashed line shows the contribution from Russian rivers alone. Discharge data are from the University of New Hampshire Global Runoff Data Centre Composite Runoff Fields V1.0 (http://www.grdc.sr.unh.edu/index.html), compiled on the basis of long-term monitoring at river gauging stations dating from at least the late 1970s to the mid-1990s (ref. 50).

of dissolved Hg^0 formation across the Arctic[10,24]. We tested this hypothesis with sensitivity study (simulation 4) setting the biotic reduction rate constant to an aseasonal maximum observed value of 2.8×10^{-5} s^{-1} (ref. 25), about 100 times larger than the global mean value in GEOS-Chem[14]. Results in Fig. 2 (orange dotted line) show that this simulation overestimates atmospheric Hg^0 in winter, which may reflect the assumed aseasonality, but more importantly it still fails to sustain the observed summer maximum.

A potential source from circumpolar rivers

We conclude from the above sensitivity studies that the model must be missing a large seasonal source of mercury to the Arctic Ocean mixed layer in spring–summer and propose that large circumpolar rivers could provide much of that missing source. Rivers are regionally important sources of mercury to other ocean regions, including the Mediterranean Sea and the northern mid-latitude Atlantic[22]. Three of the ten largest rivers in the world are located in the Eurasian Arctic, drawing from large drainage basins and discharging into the small and shallow Arctic Ocean[26]. The flow from circumpolar rivers to the Arctic Ocean accounts for 11% of freshwater inputs to all oceans of the world[27]. These rivers provide a major source of organic carbon to the Arctic Ocean[27] and may also be an important source of mercury as boreal soils and peatlands in catchment basins are highly enriched in stored mercury[28]. Gold, silver and mercury mines in Siberia (http://minerals.usgs.gov/minerals/pubs/country/maps/94349.gif) may also provide a large local source of mercury to Russian Arctic rivers.

As shown in Fig. 4, the seasonal cycle of Arctic freshwater discharge from rivers strongly peaks in early summer following ice break-up. In the Mackenzie River, concentrations of both dissolved and particulate mercury are up to seven times larger during peak flow than later in the year, reflecting increased mercury mobility in drainage-basin soils[29]. As a result, riverine mercury fluxes (the product of mercury concentration and water discharge volume) are up to an order of magnitude larger in early summer than during the rest of the year. The freshwater discharged by rivers remains at the surface of the stratified Arctic Ocean. Combined, these factors suggest that rivers could provide a large seasonal source of Arctic Ocean mercury.

Table 1 | Comparison between observed and modelled parameters in the Arctic Ocean.

	Reference	Months	Location of observations	Observed mean ± s.d.	Modelled mean (70°–90° N)
Ocean [Hg^0]	Ref. 12	Jul.–Sept.	Arctic Ocean	0.22 ± 0.11 pM	0.21 pM
Ocean [Hg^0]	Ref. 23*†	Aug.–Sept.	Canadian Arctic	0.13 ± 0.05 pM	0.20 pM
Ocean [THg]	Ref. 23*†	Aug.–Sept.	Canadian Arctic	2.9 ± 2.9 pM	2.5 pM
Hg^0 evasion flux	Ref. 23*	Aug.–Sept.	Canadian Arctic	87 ± 102 ng m^{-2} d^{-1}	44 ng m^{-2} d^{-1}
[Hg^0]/[THg]	Ref. 23*	Aug.–Sept.	Canadian Arctic	7.2 ± 4.9%	8.2%
Atmospheric [Hg^0]	Ref. 11	Jul.–Sept.	Arctic Ocean	1.72 ± 0.35 ng m^{-3}	1.86 ng m^{-3}
Ocean [Hg^0]	This study‡	Jun.–Jul.	n/a	n/a	0.25 pM
Ocean [THg]	This study‡	Jun.–Jul.	n/a	n/a	3.0 pM

*We include here only the subset of observations from Arctic latitudes north of 68° N (sites 1-11). †Ocean mercury concentrations refer to the surface water concentrations measured in ref. 23. ‡Arctic Ocean mercury concentrations have not been measured during early summer (Jun.–Jul.). Modelled values are nonetheless given here to show the seasonal maximum in predicted [Hg^0] and [THg]. n/a, not applicable.

Previous estimates of the annual riverine mercury flux to the Arctic Ocean range from 5 to 39 Mg yr^{-1} but are based on very limited data[30,31]. In each of the three largest Arctic rivers, all in Russia (Yenisei, Lena and Ob), mercury concentrations have been measured only once, all in the early 1990s and all in September[30], several months after expected peak concentrations. Climate change since that time has increased freshwater discharge[32] and mercury mobilization (permafrost thaw, biogeochemical activity in soil), with expected impacts for riverine mercury concentrations[33]. The limited sampling of Arctic rivers leads to very large uncertainties in the estimated mercury fluxes, even for the better-studied North American rivers. Observations rarely capture the episodic, high-intensity storm events resulting in most mercury discharge, and inferring annual fluxes from such discrete sampling data leads to significant flux underestimates[34] (see Supplementary Information).

A smaller contribution to the missing source may come from coastal erosion, particularly along the northeast Siberian coast. Erosion takes place mainly in summer, when storm-driven waves in open water can act on coastal sediments[35], but is not expected to peak until early autumn when storms are most intense[36]. As a result of this seasonal offset, erosion alone cannot replenish the ocean mercury lost to the subsurface in spring. Estimating an annual flux from coastal erosion is challenging as there are no comprehensive data on mercury concentrations in coastal sediments (observations are limited to a single set of cores from the Beaufort coast[37]). Instead, we estimate the erosion contribution based on the better-constrained organic carbon budget. Coastal erosion accounts for up to 15% of the total annual organic carbon flux to the Arctic Ocean, with the rest coming from rivers[38].

To determine the importance of these terrigenous sources in the model, we conducted a sensitivity simulation (simulation 5) that included a further source of Hg^{II} to the Arctic Ocean with expected riverine seasonality as shown in Fig. 3b (water flow seasonality of Fig. 4 compounded by riverine mercury concentrations three times higher in May–June than in the rest of the year[39]). The source from coastal erosion would probably be shifted later in the summer and we discuss the implications below. As the model does not include lateral transport in the ocean, the mercury source is applied uniformly across the Arctic Ocean. The sensitivity to this assumption is discussed in the Supplementary Information. This mercury is then available for evasion from the ocean mixed layer in areas without continuous sea-ice cover (see Supplementary Information) and subsequent atmospheric transport.

We find from this sensitivity simulation that an annual flux of 95 Mg yr^{-1} Hg^{II} to the open ocean can provide sufficient mercury to the ocean mixed layer to counteract losses to the subsurface (Fig. 3b), thereby sustaining the summer maximum in ocean evasion apparent in the atmospheric observations (blue line in Fig. 2). The model still shows a peak in June rather than July but this could reflect a delay in mercury transport from the river mouths to offshore waters as well as an offset in the timing of coastal erosion fluxes. Our estimated flux is inferred from the atmospheric observations and reflects the THg input to the open ocean needed to drive evasion.

Assuming that the partitioning between rivers and coastal erosion is the same for mercury as for organic carbon (85:15; ref. 38), our total terrigenous flux of 95 Mg yr^{-1} might be partitioned into 80 Mg yr^{-1} from rivers and 15 Mg yr^{-1} from coastal erosion. Translating these fluxes to concentrations is non-trivial owing to the uncertain seasonality of the coastal erosion contribution, but we can estimate an upper limit for rivers by assuming they account for the entire flux in early summer, leading to a maximum unfiltered riverine [THg] = 48 ng l^{-1} in June. Limited measurements in Russian rivers showed much lower concentrations, but these samples are not representative of the episodic flood events that drive most riverine transport, as discussed in the Supplementary Information. For coastal erosion, assuming a total annual sediment flux of 430 Mt yr^{-1} (ref. 38), our estimated sediment concentration of [THg] = 32 ng g^{-1} is within the range measured along the Beaufort coast (26–303 ng g^{-1}; ref. 37).

Our hypothesis of a dominant riverine source to explain the summer mercury maximum in the Arctic atmosphere is consistent with Lagrangian model analyses for Zeppelin[8] showing that the highest summer atmospheric concentrations are associated with an Arctic Ocean source. Closer examination of the source attribution maps in ref. 8 shows hotspots in the outflow basins of the Ob, Yenisei and Kolyma rivers. We conducted further back trajectory analyses with the National Oceanic and Atmospheric Administration HYSPLIT model (https://ready.arl.noaa.gov/HYSPLIT.php) and find frequent summertime transport to Alert from the central Arctic Ocean and the Eurasian shelf regions as well as transport to Amderma from the outflow regions of the nearby Russian rivers. Inclusion of the riverine source also improves model agreement with mercury measurements in the Arctic Ocean. Mean simulated summer [Hg^0] = 0.21 pM and [THg] = 2.5 pM compare well to July–September observations from across the Arctic Ocean with mean [Hg^0] = 0.22 ± 0.11 pM (ref. 12) and to August–October observations from the Canadian Arctic Archipelago with [Hg^0] = 0.13 ± 0.06 pM and [THg] = 2.8 ± 3.1 pM (ref. 23). Further comparisons to observations are shown in Table 1.

Implied budget of Arctic mercury

Figure 5 shows the annual GEOS-Chem model budget of mercury in the Arctic surface ocean–atmosphere–cryosphere system (70°–90° N), including a source of 95 Mg yr^{-1} from Arctic rivers and coastal erosion. This source dominates the input of mercury to the Arctic surface ocean. In comparison, atmospheric deposition contributes 25 Mg yr^{-1} directly to the open ocean and 20 Mg yr^{-1}

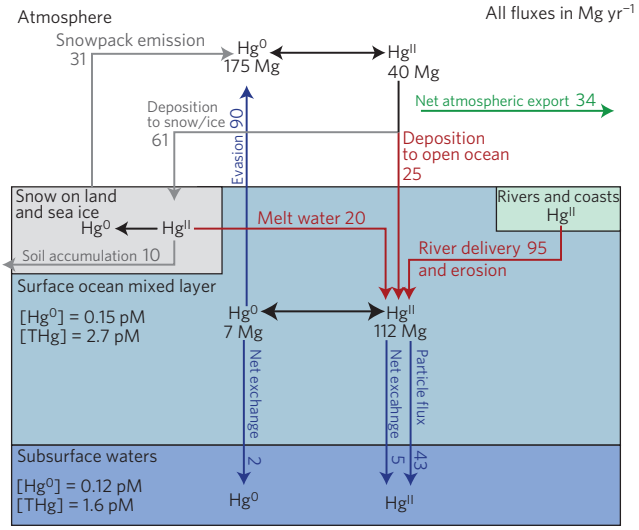

Figure 5 | Budget of mercury in the high Arctic. Annual budget of mercury for the Arctic surface ocean–atmosphere–cryosphere system (70°–90° N) as simulated by GEOS-Chem including the source from circumpolar rivers and coastal erosion. Red arrows show net inputs to the ocean mixed layer, blue arrows show net removal from the ocean mixed layer, grey arrows show atmosphere–cryosphere fluxes, black arrows show partitioning between species and the green arrow shows net atmospheric export to mid-latitudes. Also shown are modelled Hg^0 and THg concentrations for the ocean. Deposition to ice-free land (<1 Mg yr^{-1}) is not shown.

by meltwater runoff following deposition to snow on sea ice. Net annual Hg^0 evasion from the ocean to the atmosphere is 90 Mg yr^{-1}. On an annual basis, entrainment and detrainment fluxes between the surface and subsurface waters are roughly balanced, and net transport to the subsurface is mainly by particle settling. There are however large seasonal fluxes driven by entrainment/detrainment as seen in Fig. 3b. Modelled annual mean mercury concentrations in the Arctic Ocean mixed layer are [THg] = 2.7 pM and [Hg^0] = 0.15 pM, consistent with the limited observations discussed above. More data are thus urgently needed to better quantify the riverine source of mercury to the Arctic Ocean and resolve the many uncertainties in the mercury budget.

The rapid climate change taking place at present in the Arctic is probably altering the riverine mercury source to the Arctic Ocean through changes in watershed dynamics (surface hydrology, mercury mobility, soil biogeochemistry). Mercury stored in boreal soils is becoming increasingly mobilized by thawing permafrost[40] and boreal wildfires[41], and rates of river discharge are increasing[32]. In a follow-up study we will examine how changes in river flow, sea-ice cover and other climate parameters may have affected mercury trends in the Arctic over the past 30 years.

Methods

Model description. We use the GEOS-Chem v9-01-01 mercury simulation (http://geos-chem.org). The simulation is driven by Modern Era Retrospective-analysis for Research and Applications (MERRA) assimilated meteorological data from the Global Modeling and Assimilation Office Goddard Earth Observing System, produced at 0.5° × 0.667° horizontal resolution but downgraded here to 4° × 5° for input to GEOS-Chem. The MERRA data have 3-h temporal resolution for atmospheric variables and 1-h resolution for surface variables (including boundary layer height, surface temperature and sea-ice coverage). Fractional sea-ice coverage in MERRA is based on the climatology of ref. 42. The GEOS-Chem atmospheric mercury simulation is described in detail in ref. 13. The simulation includes speciated mercury emissions from both natural and anthropogenic sources, as described in ref. 43. Hg^0 in the atmosphere is oxidized by Br atoms, with Br concentrations specified by photochemical steady state with a global distribution of BrO concentrations from the p-TOMCAT model. Atmospheric Hg^{II} is partitioned between the gas and aerosol phases, photoreduces to Hg^0 in clouds and deposits by wet and dry processes[43].

The ocean mixed layer simulation is dynamically coupled to the atmosphere on the 4° × 5° grid scale and 1-h time steps as described in ref. 14. It includes atmospheric input (deposition) of Hg^{II}, exchange of Hg^0 with the atmosphere, exchange with the subsurface waters (see Supplementary Information), partitioning between dissolved and particulate Hg^{II}, and redox Hg^0/Hg^{II} chemistry by photochemical, biological and thermal processes. Ocean processes are computed in all ocean grid boxes, regardless of sea-ice cover, except evasion of Hg^0 to the atmosphere, which occurs only from ocean grid boxes with less than 100% sea-ice cover (see Supplementary Information). The ocean model does not include lateral transport. Oceanic and riverine THg concentrations and loads reported here are equivalent to those measured in environmental samples. We assume that a fraction of the oceanic (non-Hg^0) THg load is reducible. We do not explicitly simulate methylated mercury speciation (planned for a future version of the model), which will affect species partitioning but will not change the overall pool of THg available for reduction.

Bromine chemistry over polar sea ice. Relative to previous versions of GEOS-Chem[13,14], our simulation includes an improved representation of polar sea ice (from the MERRA assimilated meteorological data archive) and its implications for bromine chemistry. We assume that a polar 4° × 5° grid square in GEOS-Chem can generate BrO_x radicals in spring if at least 50% of its native resolution (0.5° × 0.667°) grid squares have more than 10% sea ice and if incident shortwave radiation at the surface is greater than 100 W m^{-2} (ref. 44). Under these conditions and on the basis of the ship and aircraft observations in refs 44,45 in the Arctic in March–April, we specify boundary layer BrO concentrations as a function of MERRA air temperature at 2-m altitude (T) as [BrO] = 20 pptv for $T \leq 248$ K, 10 pptv for $248 < T \leq 253$ K, and 5 pptv for $253 < T \leq 268$ K. Br concentrations are then calculated assuming photochemical steady state, as described previously[13]. The springtime window for BrO_x generation is defined to be February–June in the Arctic and August–December in the Antarctic on the basis of BrO column data from the GOME2 satellite (http://bro.aeronomie.be/level3_monthly.php).

Snowpack photo-reduction and re-emission. Our simulation includes an improved treatment for the fate of Hg^{II} deposited to snow. Photo-reduction of deposited Hg^{II} followed by Hg^0 re-emission is known to take place[19] but not all deposited Hg^{II} is easily reduced[18]. Observational estimates of the reducible component of Hg^{II} range from less than 10% (ref. 46) to more than 90% (ref. 19). Here we assume that 60% of deposited Hg^{II} is reducible as in ref. 13 but test the sensitivity to this assumption. Previous versions of GEOS-Chem used a temperature-based threshold to determine whether photo-reduction and re-emission occurred[13], but this resulted in spring depletion that was too weak in our simulations. In the present implementation, we assume that Hg^{II} photo-reduction for the reducible component is a first-order process with rate constant $k = 2.5 \times 10^{-9} R\ s^{-1}$, where R is the incident solar radiation at the surface in watts per square metre. The coefficient was chosen to optimize the simulation of Hg^0 in spring. For $R = 100$ W m^{-2} it implies $k = 1 \times 10^{-3}$ h^{-1}, in the mid-range of the large spread of observed estimates ranging from 7×10^{-6} to 0.6 h^{-1} (ref. 18). At snowmelt, the entire accumulated non-reducible pool as well as the remaining reducible pool is eluted with the melt water[46] and transferred to the underlying ocean or land. Hg^0 re-emitted from the snowpack following photo-reduction is added to the atmospheric reservoir, where it is available for all standard atmospheric processes (for example oxidation, deposition, transport).

Received 1 November 2011; accepted 17 April 2012; published online 20 May 2012

References

1. Steffen, A., Schroeder, W., Macdonald, R., Poissant, L. & Konoplev, A. Mercury in the Arctic atmosphere: An analysis of eight years of measurements of GEM at Alert (Canada) and a comparison with observations at Amderma (Russia) and Kuujjuarapik (Canada). *Sci. Total Environ.* **342,** 185–198 (2005).
2. Berg, T., Aspmo, K. & Steinnes, E. Transport of Hg from Atmospheric mercury depletion events to the mainland of Norway and its possible influence on Hg deposition. *Geophys. Res. Lett.* **35,** L09802 (2008).
3. Cole, A. S. & Steffen, A. Trends in long-term gaseous mercury observations in the Arctic and effects of temperature and other atmospheric conditions. *Atmos. Chem. Phys.* **10,** 4661–4672 (2010).
4. Selin, N. E. *et al.* Chemical cycling and deposition of atmospheric mercury: Global constraints from observations. *J. Geophys. Res.* **112,** D02308 (2007).
5. Steffen, A. *et al.* A synthesis of atmospheric mercury depletion event chemistry in the atmosphere and snow. *Atmos. Chem. Phys.* **8,** 1445–1482 (2008).
6. Ariya, P. A. *et al.* The Arctic: A sink for mercury. *Tellus B* **56,** 397–403 (2004).
7. Lindberg, S. E. *et al.* Dynamic oxidation of gaseous mercury in the Arctic troposphere at polar sunrise. *Environ. Sci. Tech.* **36,** 1245–1256 (2002).
8. Hirdman, D. *et al.* Transport of mercury in the Arctic atmosphere: Evidence for a spring- time net sink and summer-time source. *Geophys. Res. Lett.* **36,** L12814 (2009).

9. Kirk, J. L., St. Louis, V. L. & Sharp, M. J. Rapid reduction and reemission of mercury deposited into snowpacks during atmospheric mercury depletion events at Churchill, Manitoba, Canada. *Environ. Sci. Tech.* **40,** 7590–7596 (2006).
10. Aspmo, K. *et al.* Mercury in the atmosphere, snow and melt water ponds in the North Atlantic Ocean during Arctic summer. *Environ. Sci. Tech.* **40,** 4083–4089 (2006).
11. Sommar, J., Andersson, M. E. & Jacobi, H-W. Circumpolar measurements of speciated mercury, ozone and carbon monoxide in the boundary layer of the Arctic Ocean. *Atmos. Chem. Phys.* **10,** 5031–5045 (2010).
12. Andersson, M., Sommar, J., Gårdfeldt, K. & Lindqvist, O. Enhanced concentrations of dissolved gaseous mercury in the surface waters of the Arctic Ocean. *Mar. Chem.* **110,** 190–194 (2008).
13. Holmes, C. D. *et al.* Global atmospheric model for mercury including oxidation by bromine atoms. *Atmos. Chem. Phys.* **10,** 12037–12057 (2010).
14. Soerensen, A. L. *et al.* An improved global model for air–sea exchange of mercury: High concentrations over the North Atlantic. *Environ. Sci. Tech.* **44,** 8574–8580 (2010).
15. Bullock, O. R. Jr *et al.* The North American Mercury Model Intercomparison Study (NAMMIS): Study description and model-to-model comparisons. *J. Geophys. Res.* **113,** D17310 (2008).
16. Task Force on Hemispheric Transport of Air Pollution. Hemispheric Transport of Air Pollution 2010 Part B: Mercury. (Economic Commission for Europe, 2010).
17. Steen, A. *et al.* Natural and anthropogenic atmospheric mercury in the European Arctic: A fractionation study. *Atmos. Chem. Phys.* **11,** 6273–6284 (2011).
18. Durnford, D. & Dastoor, A. The behavior of mercury in the cryosphere: A review of what we know from observations. *J. Geophys. Res.* **116,** D06305 (2011).
19. Poulain, A. J. *et al.* Redox transformations of mercury in an Arctic snowpack at springtime. *Atmos. Environ.* **38,** 6763–6774 (2004).
20. De Boyer Montégut, C., Madec, G., Fischer, A. S., Lazar, A. & Iudicone, D. Mixed layer depth over the global ocean: An examination of profile data and a profile-based climatology. *J. Geophys. Res.* **109,** C12003 (2004).
21. Toole, J. M. *et al.* Influences of the ocean surface mixed layer and thermohaline stratification on Arctic Sea ice in the central Canada Basin. *J. Geophys. Res.* **115,** C10018 (2010).
22. Sunderland, E. M. & Mason, R. P. Human impacts on open ocean mercury concentrations. *Glob. Biogeochem. Cy.* **21,** GB4022 (2007).
23. Kirk, J. L. *et al.* Methylated mercury species in marine waters of the Canadian high and sub Arctic. *Environ. Sci. Tech.* **42,** 8367–8373 (2008).
24. Poulain, A. J. *et al.* Potential for mercury reduction by microbes in the high arctic. *Appl. Environ. Microb.* **73,** 2230–2238 (2007).
25. Amyot, M., Gill, G. A. & Morel, F. M. M. Production and loss of dissolved gaseous mercury in coastal seawater. *Environ. Sci. Tech.* **31,** 3606–3611 (1997).
26. Vörösmarty, C. J., Fekete, B. M., Meybeck, M. & Lammers, R. B. Global system of rivers: Its role in organizing continental land mass and defining land-to-ocean linkages. *Glob. Biogeochem. Cy.* **14,** 599–621 (2000).
27. Dittmar, T. & Kattner, G. The biogeochemistry of the river and shelf ecosystem of the Arctic Ocean: A review. *Mar. Chem.* **83,** 103–120 (2003).
28. Grigal, D. Mercury sequestration in forests and peatlands: A review. *J. Environ. Qual.* **32,** 393–405 (2003).
29. Leitch, D. R. *et al.* The delivery of mercury to the Beaufort Sea of the Arctic Ocean by the Mackenzie River. *Sci. Total Environ.* **373,** 178–195 (2007).
30. Coquery, M., Cossa, D. & Martin, J. The distribution of dissolved and particulate mercury in three Siberian estuaries and adjacent Arctic coastal waters. *Wat. Air Soil Pollut.* **80,** 653–664 (1995).
31. Outridge, P., Macdonald, R., Wang, F., Stern, G. & Dastoor, A. A mass balance inventory of mercury in the Arctic Ocean. *Environ. Chem.* **5,** 89–111 (2008).
32. Shiklomanov, A. I. & Lammers, R. B. Record Russian river discharge in 2007 and the limits of analysis. *Environ. Res. Lett.* **4,** 045015 (2009).
33. Schuster, P. F. *et al.* Mercury export from the Yukon River basin and potential response to a changing climate. *Environ. Sci. Tech.* **45,** 9262–9267 (2011).
34. Walling, D. & Webb, B. Estimating the discharge of contaminants to coastal waters by rivers: Some cautionary comments. *Mar. Pollut. Bull.* **16,** 488–492 (1985).
35. Lantuit, H. Fifty years of coastal erosion and retrogressive thaw slump activity on Herschel Island, southern Beaufort Sea, Yukon Territory, Canada. *Geomorphology* **95,** 84–102 (2008).
36. Atkinson, D. E. Observed storminess patterns and trends in the circum-Arctic coastal regime. *Geo.-Mar. Lett.* **25,** 98–109 (2005).
37. Leitch, D. R. *Mercury Distribution in Water and Permafrost of the Lower Mackenzie Basin, Their Contribution to the Mercury Contamination in the Beaufort Sea Marine Ecosystem, and Potential Effects of Climate Variation* Master of Science thesis, Univ. Manitoba (2006).
38. Rachold, V. *et al.* in *The Organic Carbon Cycle in the Arctic Ocean* (eds Stein, R. & Macdonald, R.) Ch. 2, 33–55 (Springer, 2004).
39. Graydon, J. A., Emmerton, C. A., Lesack, L. F. W. & Kelly, E. N. Mercury in the Mackenzie River delta and estuary: Concentrations and fluxes during open-water conditions. *Sci. Total Environ.* **407,** 2980–2988 (2009).
40. Rydberg, J., Klaminder, J., Rosén, P. & Bindler, R. Climate driven release of carbon and mercury from permafrost mires increases mercury loading to sub-arctic lakes. *Sci. Total Environ.* **408,** 4778–4783 (2010).
41. Turetsky, M. R. *et al.* Wildfires threaten mercury stocks in northern soils. *Geophys. Res. Lett.* **33,** L16403 (2006).
42. Reynolds, R. W., Rayner, N. A., Smith, T. M., Stokes, D. C. & Wang, W. An improved *in situ* and satellite SST analysis for climate. *J. Clim.* **15,** 1609–1625 (2002).
43. Amos, H. A. *et al.* Gas-particle partitioning of atmospheric Hg(II) and its effect on global mercury deposition. *Atmos. Chem. Phys.* **12,** 591–603 (2012).
44. Pöhler, D., Vogel, L., Frieß, U. & Platt, U. Observation of halogen species in the Amundsen Gulf, Arctic, by active long-path differential optical absorption spectroscopy. *Proc. Natl Acad. Sci. USA* **107,** 6582–6587 (2010).
45. Prados-Roman, C. *et al.* Airborne DOAS limb measurements of tropospheric trace gas profiles: Case studies on the profile retrieval of O4 and BrO. *Atmos. Meas. Tech.* **4,** 1241–1260 (2011).
46. Dommergue, A. *et al.* The fate of mercury species in a sub-arctic snowpack during snowmelt. *Geophys. Res. Lett.* **30,** 1621 (2003).
47. Weiss-Penzias, P., Jaffe, D. A., McClintick, A., Prestbo, E. M. & Landis, M. S. Gaseous elemental mercury in the marine boundary layer: Evidence for rapid removal in anthropogenic pollution. *Environ. Sci. Tech.* **37,** 3755–3763 (2003).
48. Sigler, J. M., Mao, H. & Talbot, R. Gaseous elemental and reactive mercury in Southern New Hampshire. *Atmos. Chem. Phys.* **9,** 1929–1942 (2009).
49. Yatavelli, R. L. N. *et al.* Mercury, PM2.5 and gaseous co-pollutants in the Ohio River Valley region: Preliminary results from the Athens supersite. *Atmos. Environ.* **40,** 6650–6665 (2006).
50. Fekete, B. M., Vörösmarty, C. J. & Grabs, W. Global, composite runoff fields based on observed river discharge and simulated water balances. (Univ. New Hampshire and Global Runoff Data Centre, 2000).

Acknowledgements

This work was financially supported by the Arctic System Science Program of the US National Science Foundation. Financial support for the Alert and Amderma data sets was provided by the Northern Contaminants Program, Environment Canada and the Arctic Monitoring and Assessment Programme. We thank A. Cole for providing the Alert data; A. Konoplev and F. Pankratov at SPA Typhoon in Obninsk, Russia for providing the Amderma data; K. A. Pfaffhuber, T. Berg and the Chemical Co-ordinating Centre of EMEP for providing the Zeppelin data; and E. Corbitt and C. Holmes for helpful conversations.

Author contributions

J.A.F. designed, performed and interpreted the model simulations. D.J.J. and E.M.S. supervised the research and contributed significantly to interpretation of the results. A.L.S. and H.M.A. developed major components of the model. A.S. collected the Alert data. J.A.F. wrote the paper, and all authors edited and revised the paper.

Additional information

The authors declare no competing financial interests. Supplementary information accompanies this paper on www.nature.com/naturegeoscience. Reprints and permissions information is available online at www.nature.com/reprints. Correspondence and requests for materials should be addressed to J.A.F.